Available online at www.sciencedirect.com
SCIENCE DIRECT
Electrochimica Acta 51 (2006) 4865–4872
ELECTROCHIMICA Acta
www.elsevier.com/locate/electacta

Li^+-intercalation electrochemical/electrochromic properties of vanadium pentoxide films by sol electrophoretic deposition

Ying Wang, Guozhong Cao *

Department of Materials Science and Engineering, University of Washington, Seattle, WA, United States

Received 4 November 2005; received in revised form 13 January 2006; accepted 13 January 2006
Available online 14 February 2006

Abstract

Thin films of orthorhombic V_2O_5 have been prepared by sol electrophoretic deposition (EPD) followed by post-treatment at 500 °C. Their electrochemical and optical performances have been investigated for possible applications in electrochemical/electrochromic devices. Li^+-intercalation properties of the films have been explored in two voltage ranges: 0.4 to −1.1 V and 0.4 to −1.6 V versus Ag/Ag^+, respectively. High capacities of over 300 mAh/g are acquired in the wider voltage range at a current density of 50 $\mu A/cm^2$ and moderate capacities of 140 and 110 mAh/g are obtained in the narrower voltage range at a current density of 25 and 50 $\mu A/cm^2$, respectively. Electrochemical measurements have shown that the films demonstrate good cyclability in both voltage ranges. X-ray diffraction, scanning electron microscopy and optical spectra have been used to examine the changes in crystallinity, microstructure, morphology and transmittance of the films during cycling. Films cycled to a deeper voltage of −1.6 V versus Ag/Ag^+ deliver higher capacity with appreciable morphological change, while films cycled in the narrower voltage range show moderate capacity and maintain the morphology, optical responses and crystalline structure. Voltage range can be optimized in between to acquire both high capacity and stability in structure, electrochemical and optical properties. High Li^+-intercalation capacity and good cyclic stability are attributed to the porous structure of V_2O_5 films prepared by EPD.

Keywords: Vanadium pentoxide film; Electrophoretic deposition; Lithium ion intercalation; Electrochemical property; Electrochromic property

1. Introduction

Electroactive films can intercalate/deintercalate guest species such as lithium ions and are used for devices such as batteries, fuel cells, and electrochromic displays [1]. Vanadium pentoxide (V_2O_5) is a typical Li^+-intercalation compound due to its layer structure [2,3]. Hence the thin film of V_2O_5 is a promising candidate for cathode in batteries [4,5] and counter electrode (in conjunction with WO_3) in electrochromic devices [6,7]. The electrochemical property of V_2O_5 film is originated from its capability to release/store the energy during Li^+-intercalation/deintercalation processes. The electrochromic property of V_2O_5 is characterized by its ability to evoke reversible and persistent changes of the optical properties upon charging/discharging [8]. V_2O_5 is special in that Li^+-intercalation makes the transmittance decrease in the near infrared and long-wavelength part of the luminous spectrum, while the transmittance increases in the short-wavelength and ultraviolet parts of this spectrum. For either electrochemical or electrochromic application, V_2O_5 film is required to have decent specific capacity and extended cycling stability.

The electrochemical/electrochromic properties of V_2O_5 have been studied in detail for films made by versatile deposition techniques ranging from high-energy, dry deposition methods to low-energy, wet methods that are more common. The high-energy techniques include thermal evaporation [9], RF magnetron sputtering [10–12], dc magnetron sputtering [13] and pulsed laser deposition [14]. The low-energy techniques, or the chemical techniques include electrochemical deposition (ECD) [15], chemical vapor deposition [16] and sol–gel deposition such as dip-coating and spin-coating [17]. The techniques that have been used to form the electroactive films usually influence their morphology, properties, and performance. The present work concerns the deposition and property study of V_2O_5 films made by sol electrophoretic deposition (EPD). The electrophoretic

* Corresponding author. Tel.: +1 206 616 9084; fax: +1 206 543 3100.
E-mail address: gzcao@u.washington.edu (G. Cao).

0013-4686/$ – see front matter © 2006 Elsevier Ltd. All rights reserved.
doi:10.1016/j.electacta.2006.01.026

deposition technique has been widely used for the film deposition of metal oxides because of the low operating temperature and low cost of the process. Furthermore, the as-deposited films have better uniformity and homogeneity than those made from other wet techniques such as spin-coating or dip-coating. Thickness of films prepared from EPD can also be more easily and precisely controlled by varying the voltage or deposition time. In comparison with other electrodeposition techniques such as electrochemical deposition (ECD), the films made from EPD have higher porosity which can be tailored by deposition conditions. Combining with sol–gel processing, our group has fabricated a variety of oxide nanorod arrays of simple, complex and doped oxides by template-based EPD [18–20]. Single-crystalline V_2O_5 nanorod arrays have been grown by combining the template-based method with either electrochemical deposition or electrophoretic deposition [21–23]. It was found that the lateral shrinkage of nanorods made from EPD (50%) was larger than that of nanorods made from ECD (0% for anodic oxidation and 15% for surface condensation induced by local pH change) [21] Although the nanostructured V_2O_5 electrode made from electrophoretic deposition has higher rate capabilities and is promising for use in compact batteries [21], electrochromic displays demand a large area of electroactive material and to date there is no practical way to synthesize a large area of nanorod arrays. Thus it is still necessary to study the processing and properties of thin films of V_2O_5. On the other hand, V_2O_5 films prepared by physical methods [12] or some chemical methods (such as electrochemical deposition [15] and chemical vapor deposition [16]) are rather dense and may have limited capacities as a result. Hence, we aim to investigate V_2O_5 films prepared from sol electrophoretic deposition which promise higher porosity and better Li^+-intercalation performance.

Electrophoretic deposition differs from electrochemical deposition in several aspects [18,24–26]. First, the materials deposited by electrophoretic deposition need not be electrically conductive. Therefore, this method is particularly useful for oxide systems. Secondly, nanosized particles in colloidal dispersions are typically stabilized by electrostatic or electrosteric mechanisms. When dispersed in a polar solvent or an electrolyte solution, the surface of nanoparticles develops an electrical charge via one or more of the following mechanisms: (1) preferential dissolution or (2) deposition of charges or charged species, (3) preferential reduction or (4) oxidation, and (5) adsorption of charged species such as polymers. Charged surfaces will electrostatically attract oppositely charged species (typically called counter-ions) in the solvent or solution. A combination of electrostatic forces, Brownian motion and osmotic forces results in the formation of the double layer structure. Upon application of an external field to a colloidal system or a sol, the constituent charged particles are set in motion in response to the electric field. This type of motion is referred to as electrophoresis. When a charged particle is in motion, some of the solvent or solution surrounding the particle will move with it, since part of the solvent or solution is tightly bound to the particle. Electrophoretic deposition simply uses such an oriented motion of charged particles to grow films or monoliths by enriching the solid particles from a colloidal dispersion or a sol onto the surface of an electrode. If particles are negatively charged, the deposition of solid particles will occur at the anode. Otherwise, deposition will be at the cathode.

This paper studies the Li^+-intercalation electrochemical/electrochromic properties of V_2O_5 films made from EPD. The relationships between the microstructure, morphology, electrochemical and optical properties of as-deposited and lithiated films are discussed.

2. Experimental

A diluted V_2O_5 sol was prepared using a method reported by Fontenot et al. [27] with V_2O_5 powder (Sigma–Aldrich) and H_2O_2 (30 wt.% in H_2O, Sigma–Aldrich) as precursor. V_2O_5 powder was dissolved in H_2O_2 solution with a V_2O_5 concentration of 0.15 M. The resulting solution has H_2O_2/V_2O_5 ratio of 8:1. After stirring for 1.5 h at room temperature, the excess H_2O_2 was decomposed by heated at 70–80 °C, and a red–brown gel was obtained. The resultant gel was then re-dispersed in DI-water, resulting in the formation of brownish sol, which contained 0.01 mol/l vanadium with a pH of 2.7. The primary vanadium species in the colloidal dispersion are nanoparticles of hydrated vanadium oxide. V_2O_5 films were prepared by electrophoretic deposition in a Teflon boat with V_2O_5 sol as the electrolyte. ITO substrate was used as the deposition electrode and Pt rod as counter electrode; the distance between these two electrodes was kept at ~3.5 cm. Deposition voltage was 5 V. The V_2O_5 particles were negatively charged in the as-prepared sol, therefore ITO substrate was used as positive electrode. The crystallization of V_2O_5 films was performed using thermal annealing in air. To avoid shrinkage of the films, the samples were first heated at 110 °C for 6 h, followed by raising temperature at a rate of 1 °C/min and the films were annealed at 500 °C in air for 1 h. Then, a slow cooling procedure to room temperature was performed in order to obtain a good adherence of the deposition of films on the substrate. All the samples have a geometric area of 1 cm^2. All the samples were stored in a desiccator before measurements.

Scanning electron microscopes (SEM, JEOL JSM-5200) was used to characterize the morphology of V_2O_5 films before and after electrochemical redox cycles. X-ray diffraction (XRD) patterns of V_2O_5 films were obtained by using a Philips PW1820 diffractometer. The diffractometer operated at 40 kV and 20 mA in the standard $\theta-2\theta$ configuration. JCPDS data cards used for the indexing of the XRD peaks are 09-0387 and 06-0416 for V_2O_5 and In_2O_3, respectively. Electrochemical properties of V_2O_5 film electrode were investigated using a standard three-electrode cell, with the 1 M-$LiClO_4$ solution in propylene carbonate as the electrolyte, a Pt mesh as the counter electrode and $Ag/AgNO_3$ as the reference electrode. Cyclic voltammetric and chronopotentiometric measurements of these films were carried out by using an electrochemical analyzer (CH Instruments, Model 605B). Optical transmittance spectra of the V_2O_5 films before and after cycling were carried out in the wavelength range of 200–900 nm using fiber optic spectrometer (Ocean Optics, Inc.).

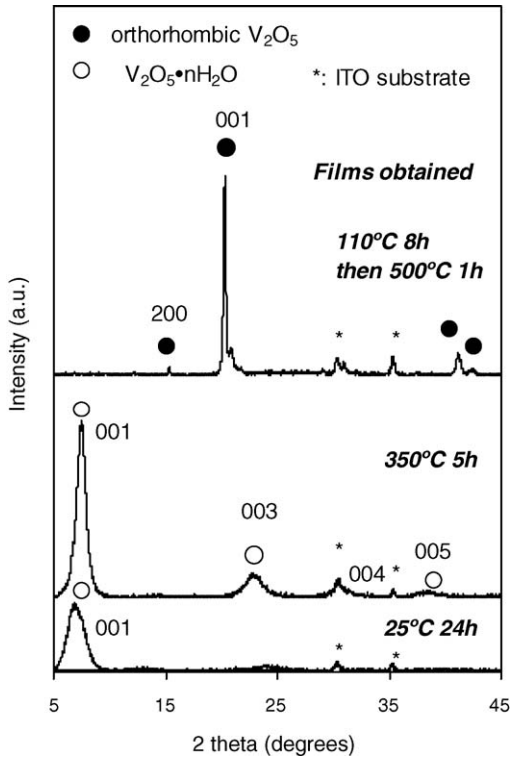

Fig. 1. X-ray diffractions patterns of vanadium pentoxide films obtained at 25, 350 and 500 °C.

3. Results and discussion

Fig. 1 presents XRD diagrams of three electrophoretically deposited films of vanadium pentoxides that are dried under ambient condition for 24 h, heated at 350 °C for 5 h, and heated at 500 °C for 1 h, respectively. The diagrams of the unheated film and the film annealed at 350 °C have broad peaks, indicating a fine-grained, or nanocrystalline nature, similar to those of $V_2O_5{\cdot}nH_2O$ xerogels reported in the literature [28]. Therefore, the films obtained at room temperature and 350 °C are composed of $V_2O_5{\cdot}nH_2O$. The most intense peak is (0 0 1) diffraction, which is related to the ribbon stacking along the *c*-axis. For the unheated film, the basal spacing along this direction is 12.79 Å which corresponds to the inter-ribbon-distance, i.e., the stacking of two V_2O_5 fibers and one single water layer [28]. For the V_2O_5 film annealed at 350 °C for 5 h, the intensity of 0 0 1 peak becomes much higher and other weak peaks such as (0 0 3) (0 0 4), and (0 0 5) become more distinct, suggesting the film structure becomes less disordered. The interlayer spacing along the *c*-axis is calculated to be 11.79 Å. Obviously the interlayer spacing shrinks because some water intercalated between adjacent layers is removed for the film during heating. It is interesting to note that the interlayer spacing, 12.79 Å for electrophoretically deposited $V_2O_5{\cdot}nH_2O$, is larger than 11.74 Å for the sol–gel deposited $V_2O_5{\cdot}nH_2O$ [29] and larger than 11.52 Å for $V_2O_5{\cdot}nH_2O$ xeorogels reported in the literature [28]. Similarly, the sol–gel deposited film of vanadium pentoxides crystallize at 330 °C [29] while the V_2O_5 film electrophoretically deposited from the same sol does not contain any crystalline phase even by heating at 350 °C as shown in Fig. 1. Such result may be ascribed to more water intercalated between the layer structure of V_2O_5 in the electric field during the electrophoretic deposition process and these water molecules expand the interlayer spacing more. The larger water content in V_2O_5 EPD films also causes the film to dehydrate and crystallize at higher temperature. After heating at 500 °C for 1 h, the $V_2O_5{\cdot}nH_2O$ film is entirely converted to a yellow crystalline thin film of orthorhombic phase, as confirmed by XRD pattern in Fig. 1. The crystallite size values, *L*, can be calculated from the broadening of the corresponding (*h k l*) lines according to the Scherrer's formula [30,31]. The crystallite size along the *a*-axis is 72.6 nm, deduced from (0 0 1) peak; and the crystallite size along the *c*-axis is 38.4 nm, deduced from (2 0 0) peak. The crystallite size along the *b*-axis is not deducible since (0 *k* 0) peak is not observed in the XRD. The cell parameters deduced from the exploitation of the XRD patterns in the case of V_2O_5-deposited films (orthorhombic system) are $a = 11.524$ Å, and $c = 4.377$ Å. Similarly, the lattice parameter *b* is not deducible because of missing of (0 *k* 0) peak in the XRD. These results are close to those given in the JCPDS card corresponding to orthorhombic V_2O_5 ($a = 11.510$ Å and $c = 4.371$ Å). The cell parameters are also similar to those reported in the literature in the case of well-crystallized V_2O_5. For example, the cell parameters for V_2O_5 obtained by the chemical vapor deposition are $a = 11.518$ Å and $c = 4.403$ Å [16]; the parameters for V_2O_5 prepared by the sol–gel method are $a = 11.512$ Å and $c = 4.371$ Å [32].

All the films grown by EPD have smooth surface morphology and are crack free prior to and after heat treatments. Fig. 2(a) shows SEM image of the orthorhombic V_2O_5 film obtained at 500 °C. Part of the film is broken off to reveal both top and cross-sectional view. It can be seen that the film is homogeneous and coherent. Fig. 2(b) presents a closer cross-sectional view when

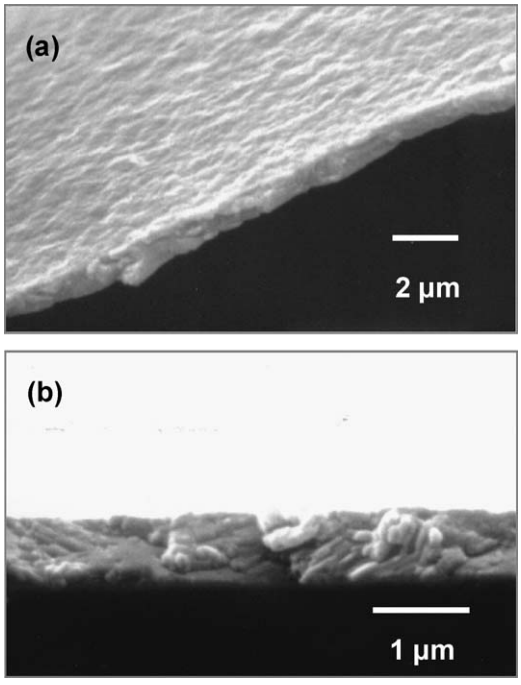

Fig. 2. SEM images of (a) orthorhombic V_2O_5 film after breakage and (b) cross-section view when the V_2O_5 film in (a) is further tilted up.

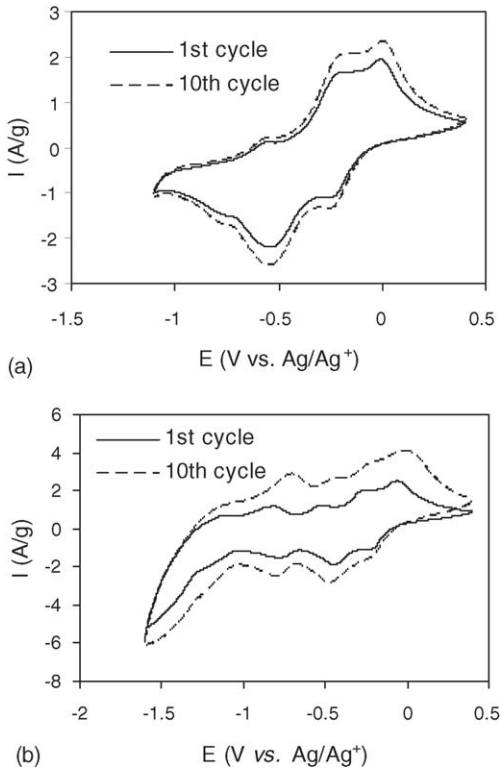

Fig. 3. (a) CV cycles of V_2O_5 films in the voltage range of 0.4 to −1.1 V. (b) CV cycles of V_2O_5 films in the voltage range of 0.4 to −1.6 V. The scan rate is 10 mV/s.

the film in (a) is further tilted up. The film thickness is estimated to be 0.8 μm.

The lithium intercalation is first investigated by cyclic voltammetry (CV) with a scan rate of 10 mV/s. V_2O_5 film made from EPD presents an electrochemically active region between 0.4 and −1.1 V versus Ag/Ag^+. The 1st and 10th CV cycles in this region are shown in Fig. 3(a). The 1st CV cycle shows two well-defined cathodic peaks at −0.21 and −0.57 V and a less distinct peak at −0.82 V, corresponding to Li^+-intercalation; it exhibits two well-defined anodic peaks at 0.03 and −0.18 V and a less distinct peak at −0.55 V, associated with Li^+ deintercalation. In the 10th cycling, the shape of CV curve is similar to the 1st cycle and there is almost no change in peak positions, although the area of the 10th CV expands slightly, indicating the electrochemical stability of the V_2O_5 film. The voltage range is further decreased to −1.6 V versus Ag/Ag^+. Fig. 3(b) shows the 1st and the 10th CV cycles of V_2O_5 film in a potential window of 0.4 to −1.6 V versus Ag/Ag^+. The shape of CV curve suggests some irreversible Li ion intercalation. However, for the short-term cycling, the 10th cycle expands in comparison with the 1st cycle, but the positions of both cathodic and anodic peaks shift distinctly. For example, the cathodic peak at −0.82 V in the 1st cycle shifts to −0.86 V in the 10th cycle. For both cycling in the 1.5-V range (0.4 V to −1.1 V) and the 2-V range (0.4 to −1.6 V), the shapes of CV curves closely resemble the voltammograms of V_2O_5 film obtained by reactive dc magnetron sputtering and cycled in a 1.5-V region and a 2-V region, respectively [12] The results are also in a good agreement with those of V_2O_5 films

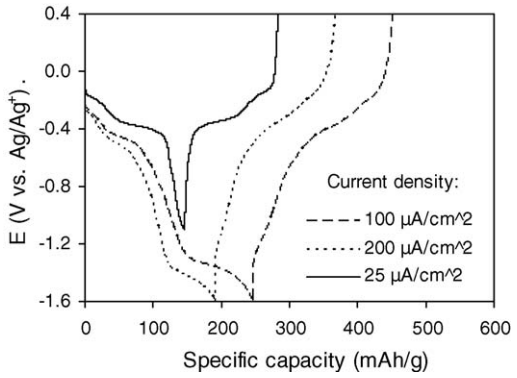

Fig. 4. Discharge–charge curves (1st cycle) of V_2O_5 films. Solid line: cycled between 0.4 and −1.1 V vs. Ag/Ag^+ at a current density of 25 $\mu A/cm^2$; dashed line: cycled between 0.4 and −1.6 V vs. Ag/Ag^+ at a current density of 100 $\mu A/cm^2$; solid line: cycled between 0.4 and −1.6 V vs. Ag/Ag^+ at a current density of 200 $\mu A/cm^2$.

prepared by evaporation [33], electrochemical deposition [34], and spin-coating [35].

The lithium intercalation property of V_2O_5 films is then studied by chronopotentiometry (CP). Fig. 4 gives the discharge–charge profiles of the V_2O_5 cathodes obtained by annealing at 500 °C. Plateaus are observed from −0.3 to −0.5 V versus Ag/Ag^+. In this voltage discharge interval the $Li_xV_2O_5$ structure undergoes phase changes, α, ε, and δ each with a different x-value of Li intercalation by comparing these plateaus to literature [36]. When cycled between 0.4 and −1.6 V versus Ag/Ag^+, the films exhibit high capacities of 250 and 190 mAh/g at current densities of 100 and 200 $\mu A/cm^2$, respectively. However, such a high capacity occurs over a wide voltage range of 2 V and cycling in this region may inflict some morphological/structural change as discussed in the CV measurements above. Accordingly, Fig. 4 also shows the discharge–charge profile of the V_2O_5 film cycled between 0.4 and −1.1 V at a current density of 25 $\mu A/cm^2$ and the V_2O_5 films delivers a capacity of 140 mAh/g. The discharge–charge curves in the 1.5-V region are more symmetric than those in the 2.0-V region, suggesting the film has more stable cyclability in the narrower voltage range.

The long-term cycling performances of the V_2O_5 films are further studied by cycling the films 50 times in the two voltage ranges, respectively. Fig. 5(a) and (b) show the first 10 discharge–charge cycles and the last 10 cycles, respectively. The film is cycled between 0.4 and −1.1 V versus Ag/Ag^+ at a current density of 100 $\mu A/cm^2$. The initial open-circuit voltage of the V_2O_5 film is about −1.8 V versus Ag/Ag^+. After delivering an intial discharge capacity of 100 mAh/g in the 1st cycle, the capacity decreases to 60 mAh/g in the 2nd cycle but slightly increases afterwards and the discharge capacity in the 50th cycle is 70 mAh/g. Similarly, Fig. 5(c) and (d) present the first 10 discharge–charge cycles and the last 10 cycles for the film cycled between 0.4 and −1.6 V at a current density of 100 $\mu A/cm^2$. The initial open circuit voltage is about −1.8 V versus Ag/Ag^+ as well. After delivering an initial capacity of 250 mAh/g in the 1st cycle, the capacity decreases to 180 mAh/g in the 2nd cycle but increases again, and the discharge capacity in the 50th cycle reaches 310 mAh/g which is even higher than the initial capacity.

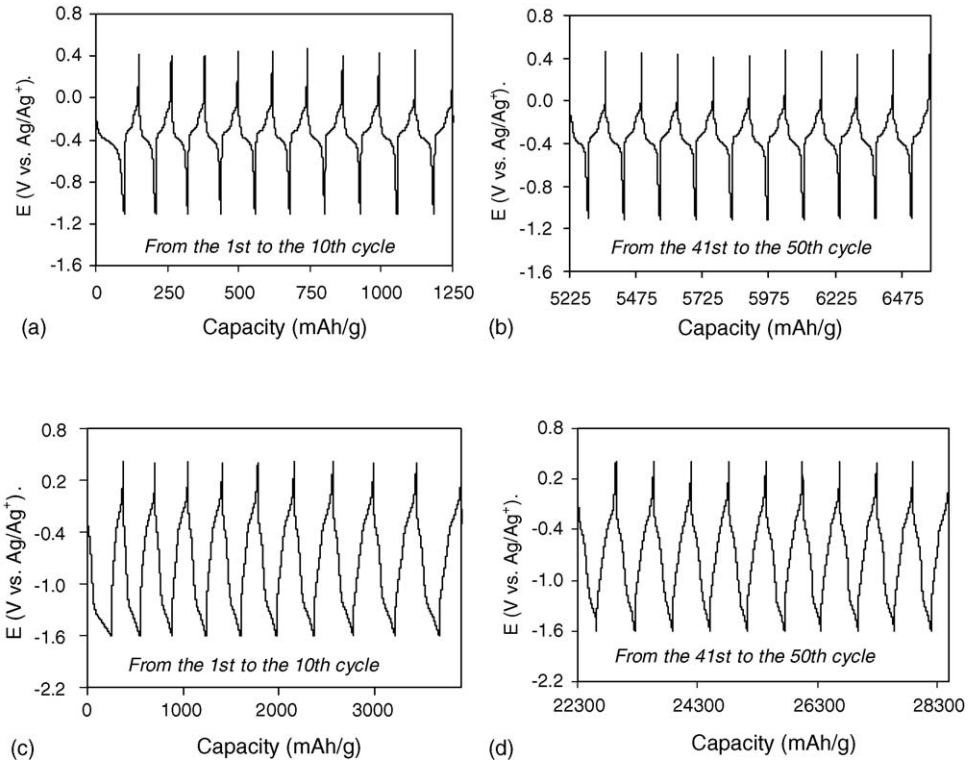

Fig. 5. Discharge–charge cycles of V_2O_5 films at a current density of 100 μA/cm^2: (a) the first 10 cycles in the voltage range of 0.4 to −1.1 V, (b) the 41st to the 50th cycles in the voltage range of 0.4 to −1.1 V, (c) the first 10 cycles in the voltage range of 0.4 to −1.6 V and (d) the 41st to the 50th cycles in the voltage range of 0.4 to −1.6 V. Voltage is vs. Ag/Ag$^+$.

It is interesting to note that cycling in the two different voltage ranges both exhibits increase in the discharge capacity from the 2nd cycle onwards; furthermore, for the V_2O_5 film cycled in the larger voltage range, the increase of capacity is more significant.

Fig. 6(a) summarizes the discharge capacities as a function of cycle number in the range of 0.4 to −1.1 V at various current densities such as 50, 100 and 200 μA/cm^2. The current densities we chose are higher or compatible with those commonly used in literature for V_2O_5 films with similar thickness to ours [13,16]. At the current density of 50 μA/cm^2, the V_2O_5 film possesses an initial discharge capacity of 110 mAh/g and reaches a discharge capacity of 80 mAh/g in the 50th cycle. At all the three current densities, the discharge capacities of the V_2O_5 film decrease first then increase starting from the 2nd cycle until reach a plateau. Fig. 6(b) gives evolution of discharge capacity in the potential window of 0.4 to −1.6 V versus Ag/Ag$^+$ at the three different current densities. At the relatively low current density of 50 μA/cm^2, the V_2O_5 film has an initial capacity of 300 mAh/g then decreases in the 2nd cycle and increases again. Within six cycles, the capacity reaches a maximum value of 380 mAh/g in the 6th cycle, followed by slight decrease with small fluctuation in the value until to the end. At the medium current density of 100 μA/cm^2, an initial decline of capacity is followed by substantial increase until a plateau is reached after 15 cycles. At the relatively large current density of 200 μA/cm^2, the capacity again drops initially then increases persistently to the end of 50 cycles. The trend of cycling performances at three different current densities looks similar, and the capacities after 50 redox cycles are all larger than the initial capacities. However, follow-

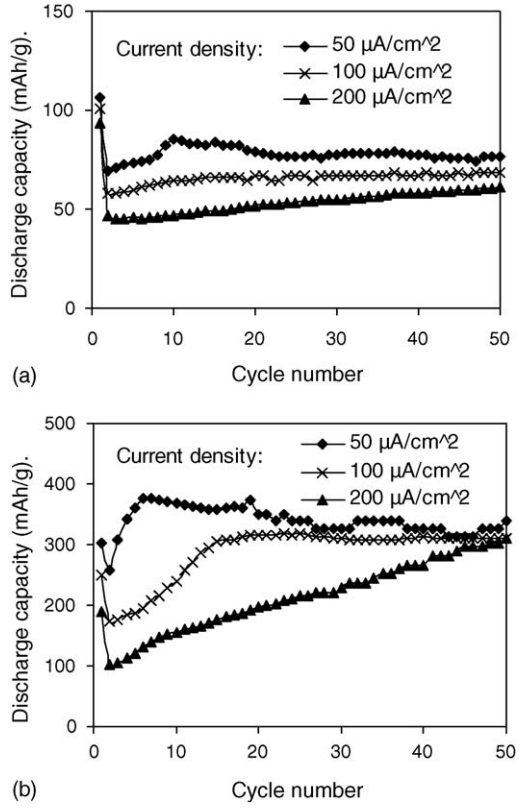

Fig. 6. Discharge capacities as a function of cycle number for V_2O_5 films cycled in the voltage ranges of (a) 0.4 to −1.1 V vs. Ag/Ag$^+$ and (b) 0.4 to −1.6 V vs. Ag/Ag$^+$.

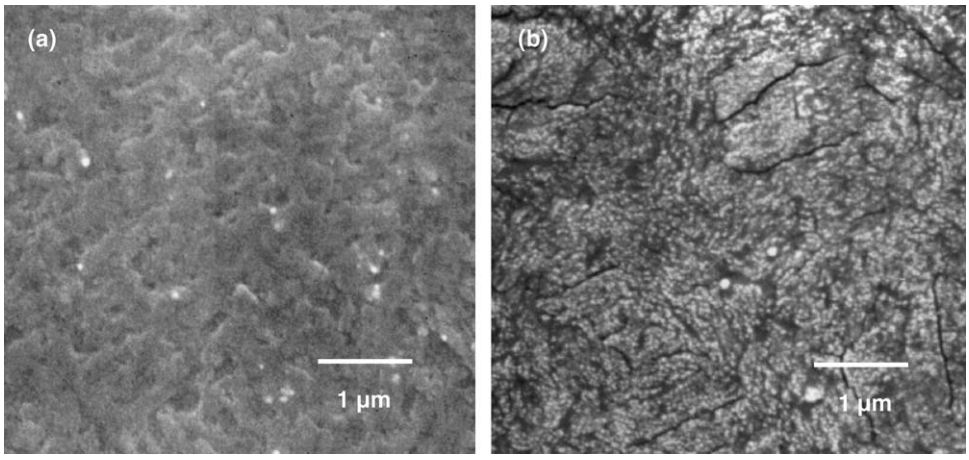

Fig. 7. SEM images of V_2O_5 films (a) before cycling and (b) after 50 redox cycles in the voltage range of 0.4 to −1.6 V vs. Ag/Ag^+ and at a current density of 100 μA/cm^2.

ing the initial degradation, the increase in the capacity value is more substantial and extends to more cycles when the current density is larger. Accordingly, for these three groups of cyclability data, the final capacities after 50 cycles are getting closer in value, despite the significant difference of initial capacities and current densities. Further, comparison between Fig. 6(b) and (a) suggests that the increase in the capacity value following initial decrease is more substantial when the film is discharged to a deeper voltage. The capacity increasing in the second cycle compared with that of the first cycle is likely due to the film cracking caused by the first cycle. The cracking or defects in the films after the first cycle allows more freedom for volumetric change during Li-ion intercalation/deintercalation and, thus, the capacity increases starting in the second cycle.

SEM has been used to study the surface morphologies and possible morphological changes of the V_2O_5 films. Fig. 7(a) and (b) show the surfaces of V_2O_5 films before and after 50 redox cycles in the potential window of 0.4 to −1.6 V versus Ag/Ag^+. It can be seen from Fig. 7(a) that the V_2O_5 film is platelet-like and uniform. However, Fig. 7(b) shows the film surface becomes rougher after cycling and cracks appear. A close look at the SEM image can find extensive z-shaped cracks along the grain boundary. These observations indicate the film is over-cycled if discharged to a deeper voltage of −1.6 V and cracks occur due to the expansion/contraction of film during the Li intercalation/deintercalation process. Whereas the cracks allows more flexibility in volume changes which leads to the substantial increase of capacity from the 2nd cycle on wards as show in Fig. 7(b). It is interesting to note that the cracks are more evenly distributed than cracks occurred on the over-cycled V_2O_5 films prepared by sol–gel deposition [29], which can explain why the cycling performance of V_2O_5 film made by EPD is better than that of sol–gel deposited film. SEM examination of the V_2O_5 film cycled between 0.4 and −1.1 V versus Ag/Ag^+ for 50 cycles shows no cracks and the cycled film looks almost the same as the virgin film. The comparison between optical responses of the virgin film and the cycled film further confirms this reversibility of Li^+-intercalation/deintercalation in the potential window of 0.4 to −1.1 V. Fig. 8 compares the ex situ optical transmittance spectra for V_2O_5 films that are before cycling, discharged to −1.1 V and after 50 redox cycles at a current density of 100 μA/cm^2, respectively. The coloration of V_2O_5 films changes progressively during the redox cycle. They turn from yellow to green, then blue upon further intercalation of Li ions. As shown in Fig. 8, transmittance change for the films between the intercalation state and deintercalation state is over 40%. In addition, the film cycled 50 times is back to bright yellow and has similar transmittance spectra as that of the virgin film. These results indicate that the electrophoretically deposited V_2O_5 films can be used for multi-colored electrochromic devices. Structural changes of the V_2O_5 films during redox cycles are further investigated by XRD. Fig. 9 presents the XRD patterns of the V_2O_5 films that are in the original state, discharged to −1.1 V, after one reduction–oxidation cycle and after 50 cycles, respectively. The films are cycled with the cut-off voltage of −1.1 V at a current density of 100 μA/cm^2. The change in the lattice parameters *a* and *c* during cycling is summarized in Table 1. Upon intercalation of Li ions, the interlayer spacing *c* increases while *a* decreases, which is consistent with the observations reported in the literature [12]. Upon the deintercalation of Li ions, the lattice parameters *a* increases and *c* decreases again, but are slightly

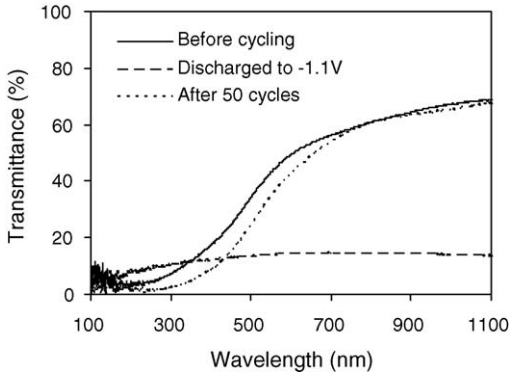

Fig. 8. Transmittance spectra for the V_2O_5 films that are before cycling, discharged to −1.1 V vs. Ag/Ag^+, and after 50 discharge–charge cycles. Cut-off voltage is −1.1 V vs. Ag/Ag^+. Current density is 100 μA/cm^2.

Table 1
Results deduced from XRD analysis for V_2O_5 films that are before cycling, discharged to −1.1 V vs. Ag/Ag^+, after 1st cycle and after 50 cycles, respectively

Film condition	2θ of 2 0 0 peak (°)	Lattice parameter *a* (Å)	2θ of 0 0 1 peak (°)	Lattice parameter *c* (Å)
Before cycling	15.365	11.5240	20.274	4.3766
Discharged to −1.1 V	15.464	11.4508	20.179	4.3970
After 1st cycle	15.449	11.4618	20.215	4.3893
After 50 cycles	15.430	11.4756	19.814	4.4771

Current density for cycling is 100 μA/cm^2.

different from the original. Therefore, there is a shift in *a* and *c* for the film cycled 50 times in comparison with the virgin film, however, the film retains the orthorhombic structure after 50 redox cycles and confirms the good cyclability. It is interesting to note that the intensity of (0 0 1) peak decreases during cycling, indicating the crystalline structure of the film gets more disordered during cycling.

Recently Mantoux et al. have synthesized orthorhombic V_2O_5 films through chemical vapor deposition (CVD) [16]. The evaluation of these V_2O_5 films revealed that the film delivered a capacity of 250 mAh/g when cycled between 3.8 and 2.2 V versus Li/Li^+ at an extremely low current density of 1.27 μA/cm^2. This current density is nearly twenty times lower than the lowest one (25 μA/cm^2) we used for cycling between 0.4 and −1.1 V versus Ag/Ag^+ and the EPD film delivers a capacity of 140 mAh/g at the current density of 25 μA/cm^2. Because of the difference in experimental conditions and current density, no precise comparison can be drawn between CVD films and EPD films, however, it can be roughly estimated that the capacities of the V_2O_5 film made from electrophoretic deposition are at least comparable with those made from CVD, or are even better if we compare the density of the film. The film made by CVD has a density close to bulk density [16], while the V_2O_5 films prepared by EPD has a density of 2.5 g/cm^3 by measuring the weight and calculating the apparent volume from the thickness revealed by the cross-section SEM image in Fig. 2(b). The porosity is thus estimated to be 25%. The pores are likely to occur during packing of the V_2O_5 platelets during electrophoretic deposition process and may shrink during sintering. As discussed earlier, the crystallite sizes along *a*- and *c*-axis are a few tens of nanometers in the film of orthorhombic phase. The pores are likely less than these crystallite sizes and thus cannot be seen in the low-magnification top view or cross-sectional view in Fig. 2. A close look at the surface morphology of V_2O_5 film reveals the porous structure as shown, in Fig. 7(a). Such porous structure allow more flexibility for volume changes during Li^+-intercalation/deintercalation processes, which attributes to the good cycling performance in both voltage ranges as shown in Fig. 6 and the good optical properties in the narrower voltage as shown in Fig. 8.

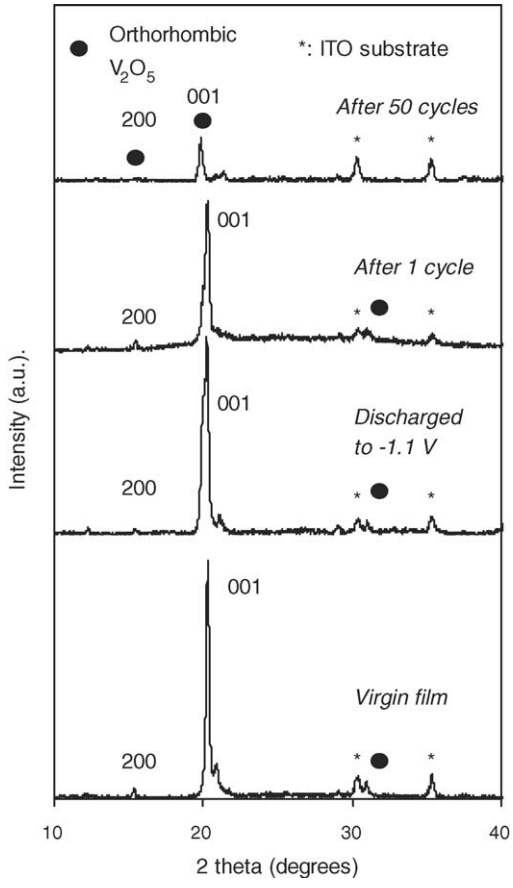

Fig. 9. XRD patterns of V_2O_5 films that are before cycling, discharged to −1.1 V vs. Ag/Ag^+, after 1 redox cycle and after 50 redox cycles, respectively. Current density for cycling is 100 μA/cm^2.

4. Conclusion

V_2O_5 thin films with thickness of 0.8 μm have been prepared through electrophoretic deposition from a sol which is made by using V_2O_5 powder and H_2O_2 as raw materials. Orthorhombic phase is acquired by heating the film at 500 °C. The electrophoretically deposited V_2O_5 films exhibit high capacities of 300 mAh/g at 0.4 to −1.6 V vs. Ag/Ag^+ at a current density of 50 μA/cm. In a narrower voltage range of 0.4 to −1.1 V vs. Ag/Ag^+, moderate capacities of 140 and 110 mAh/g are achieved at current densities of 25 and 50 μA/cm^2, respectively. The V_2O_5 films show good cyclability in both potential windows at various current densities ranging from 50 to 200 μA/cm^2. Specifically, the films cycled in the narrower voltage range of 0.4 to −1.1 V exhibit good safety characteristics as the films cycled 50 cycles retain the morphology, structure and transmittance data in comparison with the virgin film. Such high Li^+-intercalation capacity and enhanced cyclic stability are attributed to the porous structure of the V_2O_5 films by sol EPD. Not only does the porous structure offer easy Li^+ diffusion path, but also offer the needed freedom for dimension change associated with Li^+-intercalation and deintercalation process. Although films cycled in the deeper

voltage range deliver higher capacity, cracks occur along the grain boundary during cycling. For practical applications in electrochemical/electrochromic devices, an optimal voltage can be found between −1.1 and −1.6 V versus Ag/Ag^+ to realize high capacity and simultaneously retain the stability in structural and optical properties.

Acknowledgements

Y.W. acknowledges the Ford Motor Company fellowship, the graduate fellowship from PNNL-UW Joint Institute for Nanoscience (JIN), and the Nanotechnology Graduate Research Award from the University of Washington Initiative Fund (UIF). The authors are grateful for Dr. Glen E. Fryxell's valuable discussion. This work has been supported in part by National Science Foundation (DMI-0455994).

References

[1] H.K. Park, W.H. Smyrl, J. Electrochem. Soc. 141 (1994) L25.
[2] H.G. Bachmann, F.R. Ahmend, W.H. Barnes, Z. Kristallorgr. 115 (1961) 110.
[3] M.S. Whittinham, J. Electrochem. Soc. 123 (1976) 315.
[4] H.K. Park, W.H. Smryl, M.D. Ward, J. Electrochem. Soc. 142 (1995) 15.
[5] K.E. Swider-Lyons, C.T. Love, D.R. Rolison, Solid State Ionics 152–153 (2002) 99.
[6] C.G. Granqvist, Handbook of Inorganic Electrochromic Materials, Elsevier, Amsterdam, 1995.
[7] N. Özer, Thin Solid Films 305 (1997) 80.
[8] Z. Wang, J. Chen, X. Hu, Thin Solid Films 375 (2000) 238.
[9] G. Chiarello, R. Barberi, A. Amoddeo, L.S. Caputi, E. Colavita, Appl. Surf. Sci. 15 (1996) 99.
[10] S.F. Cogan, N.M. Nguyen, S.J. Perrotti, R.D.J. Rauh, Appl. Phys. 66 (1989) 1333.
[11] A. Talledo, A.M. Andersson, C.G. Granqvist, J. Appl. Phys. 69 (1991) 3261.
[12] A. Talledo, C.G. Granqvist, J. Appl. Phys. 77 (1995) 4655.
[13] C. Navone, J.P. Pereira-Ramos, R. Baddour-Hadjean, R. Salot, Proceedings of the International Workshop on Advanced Techniques for Energy Sources Investigation and Testing, Sofia, Bulgaria, September, 2004, p. 4.
[14] G.J. Fang, Z.L. Liu, Y. Wang, Y.H. Liu, K.L. Yao, J. Vac. Sci. Techol. A 19 (2001) 887.
[15] E. Potiron, A. Le Gal La Salle, S. Verbaere, Y. Piffard, D. Guyomard, Electrochim. Acta. 45 (1999) 197.
[16] A. Mantoux, H. Groult, E. Balnois, P. Doppelt, L. Gueroudjib, J. Electrochem. Soc. 151 (2004) A368.
[17] S. Passerini, D. Chang, X. Chu, D. Ba Le, W. Smyrl, Chem. Mater. 7 (1995) 780.
[18] G.Z. Cao, J. Phys. Chem. B 108 (2004) 19921.
[19] S.J. Limmer, S. Seraji, M.J. Forbess, Y. Wu, T.P. Chou, C. Nguyen, G.Z. Cao, Adv. Mater. 13 (2001) 1269.
[20] S.J. Limmer, S. Seraji, M.J. Forbess, Y. Wu, T.P. Chou, C. Nguyen, G.Z. Cao, Adv. Funct. Mater. 12 (2002) 59.
[21] K. Takahashi, S.J. Limmer, Y. Wang, G.Z. Cao, Jpn. J. Appl. Phys. 44 (2005) 662.
[22] K. Takahashi, Y. Wang, G.Z. Cao, Appl. Phys. Lett. 86 (2005) 053102.
[23] K. Takahashi, S.J. Limmer, Y. Wang, G.Z. Cao, J. Phys. Chem. B 108 (2004) 9795.
[24] I. Zhitomirsky, Adv. Colloid Interface Sci. 97 (2002) 297.
[25] O. van der Biest, L.J. Vandeperre, Annu. Rev. Mater. Sci. 29 (1999) 327.
[26] P. Sarkar, P.S. Nicholson, J. Am. Ceram. Soc. 79 (1996) 1987.
[27] C.J. Fontenot, J.W. Wiench, M. Pruski, G.L. Schrader, J. Phys. Chem. B 104 (2000) 11622.
[28] V. Petkov, P.N. Trikalitis, E.S. Bozin, S.J.L. Billinge, T. Vogt, M.G. Kanatzidis, J. Am. Chem. Soc. 124 (2002) 10157.
[29] Y. Wang, H. Shang, T. Chou, G.Z. Cao, J. Phys. Chem. B 109 (2005) 11361.
[30] L.S. Birks, H. Friedman, J. Appl. Phys. 17 (1946) 687.
[31] G.Z. Cao, Nanostructures and Nanomaterials, Synthesis, Properties and Applications, Imperial College Press, London, 2004.
[32] P. Soudan, J.P. Peirera-Ramos, J. Farcy, G. Gre'goire, N. Baffier, Solid State Ionics 135 (2000) 291.
[33] P. Baudry, M.A. Aegerter, D. Deroo, B. Valla, J. Electrochem. Soc. 138 (1991) 460.
[34] T. Yoshino, N. Baba, Y. Kouda, H. Kagaku, J. Surf. Sci. Jpn. 6 (1985) 198.
[35] K. Nagase, Y. Shimizu, N. Miura, N. Yamazoe, Appl. Phys. Lett. 60 (1992) 802.
[36] P.L. Moss, R. Fu, G. Au, E.J. Plichta, Y. Xin, J.P. Zheng, J. Power Sources 124 (2003) 261.